



Mitochondrial Calcium Nanoregulators Reverse the Macrophage Proinflammatory Phenotype Through Restoring Mitochondrial Calcium Homeostasis for the Treatment of Osteoarthritis

Xiao Lei ^{1,*}, Guodong Tan^{2,*}, Yiming Wang^{3,*}, Li Chen^{4,*}, Yuan Cao¹, Bingxin Si², Zhen Zhen², Bei Li⁵, Yan Jin⁵, Wei Wang⁶, Fang Jin ¹

¹Shaanxi Clinical Research Center for Oral Disease & Department of Orthodontics, School of Stomatology, Fourth Military Medical University, Xi'an, Shaanxi, People's Republic of China; ²Air Force Medical Center, Fourth Military Medical University, Beijing, People's Republic of China; ³Shaanxi Clinical Research Center for Oral Diseases & Department of Oral Surgery, School of Stomatology, Fourth Military Medical University, Xi'an, Shaanxi, People's Republic of China; ⁴Shaanxi Key Laboratory of Energy Chemical Process Intensification & Institute of Polymer Science in Chemical Engineering, School of Chemical Engineering and Technology, Xi'an Jiao Tong University, Xi'an, Shaanxi, People's Republic of China; ⁵State Key Laboratory of Military Stomatology & Shaanxi International Joint Research Center for Oral Diseases, Center for Tissue Engineering, School of Stomatology, Fourth Military Medical University, Xi'an, Shaanxi, People's Republic of China; ⁶State Key Laboratory of Military Stomatology & National Clinical Research Center for Oral Diseases & Shaanxi Key Laboratory of Oral Diseases, Department of Operative Dentistry and Endodontics, School of Stomatology, Fourth Military Medical University, Xi'an, Shaanxi, People's Republic of China

*These authors contributed equally to this work

Correspondence: Fang Jin, Shaanxi Clinical Research Center for Oral Disease & Department of Orthodontics, School of Stomatology, Fourth Military Medical University, Xi'an, Shaanxi, People's Republic of China. Email fangjin191@163.com; Wei Wang, State Key Laboratory of Military Stomatology & National Clinical Research Center for Oral Diseases & Shaanxi Key Laboratory of Oral Diseases, Department of Operative Dentistry and Endodontics, School of Stomatology, Fourth Military Medical University, Xi'an, Shaanxi, People's Republic of China, Email weiwang_0510@163.com

Introduction: Osteoarthritis (OA) is a chronic degenerative joint disease accompanied by an elevated macrophage proinflammatory phenotype, which is triggered by persistent pathologically elevated calcium ion levels in mitochondria. However, existing pharmacological compounds targeting the inhibition of mitochondrial calcium ion ($m[Ca^{2+}]$) influx are currently limited in terms of plasma membrane permeability and low specificity for ion channels and transporters. In the present study, we synthesized mesoporous silica nanoparticle-amidated (MSN)-ethylenebis (oxyethylenetriole)tetraacetic acid (EGTA)/triphenylphosphine (TPP)-polyethylene glycol (PEG) [METP] nanoparticles (NPs), which specifically target mitochondria and block excess calcium ion influx.

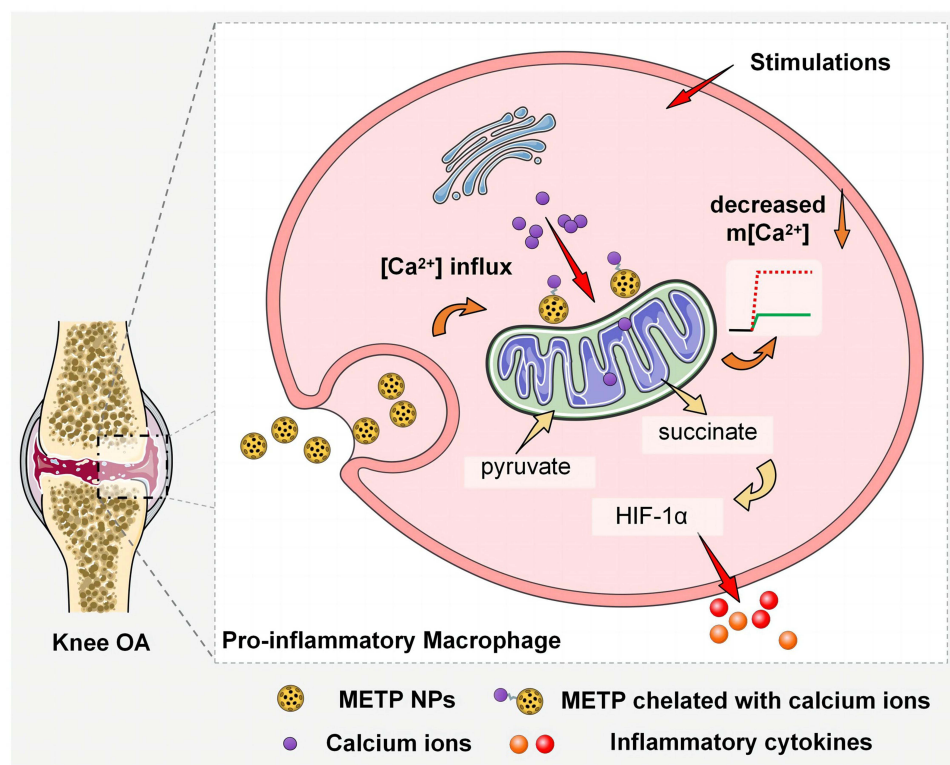
Methods: $m[Ca^{2+}]$ overload in OA mouse bone marrow-derived macrophages (BMDMs) was detected by a fluorescence probe. A tissue in situ fluorescence colocalization assay was used to evaluate METP NP uptake by macrophages. BMDMs from healthy mice were pretreated with a concentration gradient of METP NPs followed by lipopolysaccharide (LPS) stimulation and detection of $m[Ca^{2+}]$ levels in vitro. The optimal METP NP concentration was further applied, and the endoplasmic reticulum (ER) and cytoplasm calcium levels were detected. The inflammatory phenotype was measured by surface markers, cytokine secretion and intracellular inflammatory gene/protein expression. A Seahorse cell energy metabolism assay was performed to elucidate the mechanism by which METP NPs reverse the BMDM proinflammatory phenotype.

Results: The present study identified calcium overload in BMDM mitochondria of OA mice. We demonstrated that METP NPs reversed the increased $m[Ca^{2+}]$ levels in mitochondria and the proinflammatory phenotype of BMDMs, with both in vivo and in vitro experiments, via the inhibition of the mitochondrial aspartate-arginosuccinate shunt and ROS production.

Conclusion: We demonstrated that METP NPs are effective and highly specific regulators of $m[Ca^{2+}]$ overload. In addition, we demonstrated that these METP NPs reverse the macrophage proinflammatory phenotype by restoring $m[Ca^{2+}]$ homeostasis, thereby inhibiting the tissue inflammatory response and achieving a therapeutic effect for OA.

Keywords: nanoparticle, macrophage, mitochondria, calcium homeostasis, osteoarthritis

Graphical Abstract



Introduction

Osteoarthritis (OA) is a degenerative disease that can occur in all joints of the body, affecting 7% of the global population, in which persistent inflammation results in synovitis and excessive immune cell accumulation, leading to remodeling and reduced function in affected joints.^{1,2} At present, the treatment recommendation for OA is mainly concentrated on pain control and maintenance of joint function by applying non-steroidal anti-inflammatory drugs and local corticosteroid administration. However, the therapeutic effect is not ideal, and joint replacement is often the ultimate treatment. Therefore, new treatment strategies for OA, including gene therapy, extracorporeal shock wave physiotherapy, inflammation regulation and cartilage regeneration based on tissue engineering techniques,³⁻⁶ are needed.

Evidence indicates that macrophages are central to the pathophysiology of OA driving episodic cycles of chronic inflammation and tissue destruction.⁷ In OA, due to abnormal mechanical forces applied on joints, the cartilage matrix is damaged, forming matrix debris and crystals, which are then released into the synovial fluid, activating resting state macrophages towards the proinflammatory phenotype; this phenotype prompts pro-matrix metalloproteinases (p-MMPs) and cytokines, including interleukin-1 β (IL-1 β) and tumor necrosis factor- α (TNF- α), to promote cartilage destruction and subchondral bone resorption.⁸⁻¹⁰ OA patients have an increased active proinflammatory macrophage profile and few anti-inflammatory types.^{11,12}

For immune cells, such as macrophages, mitochondria are organelles not only necessary for biosynthesis and energy metabolism but also necessary for establishing and sustaining the phenotype and function of macrophages.¹³ Mitochondrial calcium ion (m[Ca²⁺]) homeostasis is essential for maintaining normal mitochondrial function and establishing inflammatory phenotypes in macrophages.¹⁴ m[Ca²⁺] overload has been reported to induce activation of proinflammatory phenotypes in macrophages by excess m[Ca²⁺] influx, which subsequently increases macrophage glycolysis,¹⁵⁻¹⁷ increases reactive oxygen species (ROS) generation^{18,19} and impairs the ability of mitochondria to buffer

intracellular calcium ion transients.^{14,20,21} However, the practicability of small molecule compounds targeting the mitochondrial calcium uniporter (MCU), such as Ru360 and TG-2112x,^{22,23} to inhibit $m[Ca^{2+}]$ influx are still limited due to shortcomings, such as permeability to the plasma membrane and low selectivity to inhibit ion channels.^{24–26}

With the extensive application of nanoparticles (NPs), the trapping and uptake of NPs by macrophages in damaged areas after administration *in vivo* has been confirmed.^{27–30} Given the ability of macrophages to aggregate and trap exogenous particles in inflammatory tissues, such as OA synovium, NPs are an ideal drug delivery targeting system. In the present study, we designed the mesoporous silica nanoparticle-amidated (MSN)-ethylenebis (oxyethylenenitrilo)tetraacetic acid (EGTA)/triphenylphosphine (TPP)-polyethylene glycol (PEG) [METP] NPs to regulate $m[Ca^{2+}]$ and phenotype in macrophages with the ability of METP NPs to target mitochondria with TPP (mitochondrial targeting agent) and consume excessive calcium ions with EGTA, a calcium ion-binding group. Herein, we demonstrated that METP NPs effectively and selectively inhibited the abnormal increase of $m[Ca^{2+}]$ in macrophages of OA mice or lipopolysaccharide (LPS)-induced cells *in vitro*. Furthermore, we demonstrated that METP NPs effectively inhibited the activation of macrophage proinflammatory phenotypes both *in vivo* and *in vitro* by downregulating glycolysis and mitochondrial aerobic respiration to reduce the production of inflammatory hypoxia-inducible factor-1 α (HIF-1 α) in the aspartate-arginosuccinate shunt and ROS generation. Elucidation of the mechanism of METP NPs fills the vacancy of drugs that inhibit $m[Ca^{2+}]$ inflow, providing a new therapeutic strategy for OA based on the regulation of macrophage $m[Ca^{2+}]$.

Materials and Methods

Chemicals

$NH_3 \cdot H_2O$ (AR, 25–28%) was purchased from Xi'an Sanpu Chemical Reagent Co., Ltd. (Xi'an, China). Aminopropyltriethoxysilane (APTES) was purchased from Energy Chemical (Shanghai, China). EGTA, trimethyl [3-(trimethoxysilyl) propyl] ammonium chloride (TMA) ($\approx 50\%$ methanol), TPP, N,N-dicyclohexyl carbonate diimide (DCC), 4-dimethylaminopyridine (DMAP), 1-(3-dimethylaminopropyl)-3-ethylcarbodiimide hydro (EDC), N-hydroxysuccinimide (NHS), and 1,3,5-trimethylbenzene (TMB) were obtained from Shanghai Macklin Biochemical Co. Tetraethylorthosilicate (TEOS, 99.0%), anhydrous tetrahydrofuran (THF) was purchased from Sinopharm Chemical Reagent Co., Ltd. (Xi'an, China). Hexadecyl trimethyl ammonium bromide (CTAB) and PEG (4000) was purchased from Tianjin Kemiou Chemical Reagent Co., Ltd. (Tianjin, China). Dimethyl sulfoxide (DMSO), toluene, hydrochloric acid, and sodium hydroxide were purchased from Tianjin HengXing Chemical Reagent Co., Ltd. (Tianjin, China). 3-bromopropionic acid was purchased from Shanghai Aladdin Bio-Chem Technology Co., LTD (Shanghai, China).

Preparation of Mesoporous Silica Nanoparticles with Large Pores and CTAB Template (MSN_T)

The preliminary MSNs were first fabricated by the classical CTAB-templated, base-catalyzed sol-gel method. Briefly, the pH value of 1000 mL deionized water was adjusted to ≈ 11 with 52.8 mL ammonium hydroxide (25–28 wt% $NH_3 \cdot H_2O$). The temperature was raised to 323 K, and then 1.12 g CTAB was added. After the CTAB was completely dissolved, 5.8 mL TEOS was added dropwise with rapid stirring. After 2 hours (h), the mixture was incubated overnight, centrifuged and washed thoroughly with distilled water and ethanol. The as-synthesized preliminary MSNs were further dispersed in ethanol by sonication for 30 minutes, followed by the addition of 20 mL of a 1:1 mixture (v/v) of water and TMB. The mixture was placed in the autoclave and kept at 140°C for 4 days without stirring. The resulting white powder was washed with ethanol and water five times each and then dried under vacuum for 20 h.

Preparation of TPP and Amino Co-Modified MSN_T (MSN_T -TPP-NH₂)

A total of 2.62 g (1 eq, 10 mmol) of TPP and 1.68 g (1.1 eq, 11 mmol) of 3-bromopropionic acid were dissolved in 20 mL of toluene and refluxed at 90°C overnight. After cooling to room temperature, the suspension was centrifuged at 12,000 rpm for 5 minutes to collect the precipitate, which was washed with toluene three times to obtain carboxyl-functionalized TPP (TPP-COOH). The resulting TPP-COOH was dissolved in 20 mL of anhydrous tetrahydrofuran (THF), and the solution was refluxed overnight at 90°C after adding 3.09 g (1.5 eq, 15 mmol) of DCC, 100 mg of DMAP,

and 2.342 mL (1 eq, 10 mol) of APTES. After cooling to room temperature and removing the insoluble substance by centrifugation, the above solution was mixed with 180 mg of as-synthesized MSNs-T, 60 μ L of APTES, and 10 mL of THF. The suspension was refluxed for 24 h at 90°C. Due to the existence of the CTAB template in the pores, modification only occurred on the surface of MSNs, resulting in TPP and amino commodified MSN_T (MSN_T-TPP-NH₂). The nanoparticles were collected by centrifuging at 12,000 rpm for 5 minutes, washed with THF five times each, and then dried under vacuum for 20 h.

Preparation of Template-Removed MSN_T-TPP-NH₂ with a Graft of TMA in the Pores (TMA-MSN-TPP-NH₂)

The surfactant template of as-synthesized MSN_T-TPP-NH₂ was removed by extraction using acidic methanol (9 mL of HCl/400 mL of methanol, 36 h) at 70°C. Afterwards, the nanoparticles were centrifuged, washed several times with ethanol, and dried under vacuum for 20 h. The resulting MSN-TPP-NH₂ was dispersed in THF containing 120 μ L of TMA, followed by overnight stirring to generate nanoparticles with TMA in the pores (TMA-MSN-TPP-NH₂). The obtained nanoparticles were washed with THF and dried in a vacuum oven at 60°C overnight.

Preparation of the Final TMA-MSN-TPP-EGTA-PEG (METP) Nano-Regulator

A total of 129.6 mg of EGTA and 54 mg of sodium hydroxide were dissolved in 10 mL of deionized water, and then 262 mg of EDC and 78 mg of NHS were added. After adjusting the pH value of the solution to 5.0, 60 mg of TMA-MSN-TPP-NH₂ was added, followed by 10 minutes of sonication. This suspension was maintained at room temperature with stirring overnight. The obtained nanoparticles (TMA-MSN-TPP-EGTA) were washed with deionized water and dried in a vacuum oven at 60°C overnight. Subsequently, the as-prepared TMA-MSN-TPP-EGTA was redispersed in 10 mL of DMSO containing EDC (786 mg), DMAP (100 mg), and PEG₄₀₀₀ (5 g). The suspension was refluxed for 4 days at 60°C. After the reaction, the suspension was cooled to room temperature, centrifuged at 12,000 rpm for 5 minutes, washed three times with deionized water, and then freeze-dried.

Microscopic Morphological Observation and Elemental Analysis of METP

The METP in powder form was resuspended in phosphate-buffered saline (PBS), dispersed by low-energy ultrasound and then dropped on copper mesh. Allow 30 seconds for METP to settle naturally on copper mesh. Absorbed excess liquid with filter paper and dried the copper mesh under a 25°C infrared lamp for 5 minutes. METP particle size and morphology were observed by an FEI Tecnai G12 Spirit BioTwin transmission electron microscope (TEM) (FEI Company, Hillsboro, Oregon, USA) with an accelerating voltage of 120 kV. For scanning electron microscope (SEM), METP in powder form was loaded on a siliceous carrier and observed surface morphology by S-4800 SEM (Hitachi, Japan), as well as elemental analysis of energy dispersive spectrum (EDS) components (Ametek EDAX, USA).

Particle Size and Zeta Potential Measurement of METP

The METP particle size was measured using Dynamic Light Scattering (DLS) and Nanoparticle Tracking Analysis (NTA) method. DLS measurements were performed with Malvern Zetasizer Nano S (Malvern, Worcestershire, UK) equipped with a 633-nm He-Ne laser at 25°C. Dispersion Technology Software version 6.01 (Malvern, Worcestershire, UK) was used to collect and analyze the data. The polydispersity index (PDI) was obtained from the autocorrelation fit of the data. For NTA measurements, the METP-PBS system was injected into the sample chamber with sterile syringes, and the particle number, size, concentration and Zeta potential were measured with the NTA NanoSight NS300 (Malvern, Worcestershire, UK) with a 633 nm laser. The NTA 3.2 software (Malvern, Worcestershire, UK) was used for capturing and analyzing the data. Three times of measurements were performed at room temperature independently.

Knee OA (KOA) Modeling and Articular Cavity Injection

Male mice of C57BL/6 strains aged 6 weeks underwent adaptive feeding firstly for 7 days, and KOA model was then established using the modified Huith method.³¹ During the operation, the medial meniscus was exposed and removed, and the anterior cruciate ligament was severed. Mice were fed and exercised normally in SPF animal room, and the injection was administered into the articular cavity during 5–8 weeks after modeling. According to the injection after modeling surgery, mice are divided randomly into 4 groups, namely the sham operation group, PBS injection group, METP treatment group and DS16570511 treatment group (n = 8). To achieve blank control, sham operation group was established by simple incision patellar ligament and sutured layer by layer. On day 28 after modeling operation, the PBS solution, METP suspension (50 µg/mL) or DS16570511 (50 µmol/L, HY-115595, MedChemExpress, USA) solution were injected into the joint cavity. A 0.3 mm × 8 mm insulin syringe (Omnican, Melsungen, Germany) was used for puncture injection of the joint cavity. The dose of each injection was 50 µL, which could be well accommodated in the joint cavity, and the injections were performed weekly for a total of 4 times. The mice were sacrificed 7 days after the fourth injection for knee joint sampling and fixed in 4% paraformaldehyde and set aside for later use. For co-localization detection of METP and macrophage marker F4/80, fluorescein isothiocyanate (FITC)-labeled METP was injected into the joint cavity and tissue sections were taken for immunofluorescence staining, and then co-localization analysis of the two fluorescence signals was performed. Joint tissue samples were divided into 3 groups according to the time node of sampling on 1st, 2nd and 3rd days after administration of FITC-labeled METP, respectively, and set aside for later staining (F4/80, ab6640, Abcam, UK).

The periodontitis (PD) modeling and drug administration methods are shown in [Supplementary Methods](#).

Extraction and Differentiation of BMDM Primary Cells

Primary bone marrow-derived macrophage (BMDM) was isolated from the bone marrow of C57 mice aged 6–8 weeks. Cells were seeded in six-well culture dishes (Corning, NY, USA) and cultured in high glucose Dulbecco's Modified Eagle's Medium (DMEM; Gibco, USA) with 10% fetal bovine serum (Hangzhou Sijiqing Biological Engineering Materials Co., Ltd. Zhejiang, China), 0.292 mg/mL L-glutamine (Invitrogen Life Technology, Carlsbad, CA, USA), 100 units/mL penicillin (Invitrogen, USA), and 100 mg/mL streptomycin (Invitrogen, USA) at 37°C with 5% CO₂. The medium was changed every 3 days. Differentiation was induced for 7 days with murine macrophage colony-stimulating factor (M-CSF, PeproTech, Rocky Hill, USA) with a concentration of 50 ng/mL added into the medium. After incubation with M-CSF, cells differentiated into resting state BMDM, which can be further induced into pro-inflammatory macrophage by LPS stimulation. Cells will not cryopreserve or passage.

F4/80 and CD11b (123,110 and 101,206, Biolegend, CA, USA) were identified by flow cytometry, and a high expression level of F4/80 and CD11b was observed, which proved that BMDM extraction and differentiation were successful ([Supplementary Figure 1A](#)).

Cell Grouping and Drug Treatment

For in vitro experiments, BMDM were divided into four groups, namely the negative control (NC) group, LPS stimulated group, METP treatment group and DS16570511 treatment group. The NC and LPS stimulated groups are BMDM without and with LPS stimulation (1 µg/mL, 12 h), respectively. In the METP treatment group, a pre-treatment period of 24 h and a concentration of 50 µg/mL are applied according to results 2.3. In the DS16570511 treatment group, the pre-treatment period of DS16570511 was 15 minutes and the concentration was 50 µmol/L (µM), assessed by m[Ca²⁺] level and BMDM surface markers CD86 and CD206 ([Supplementary Figure 1B](#) and [C](#)), which was also consistent with the methodology of Belosludtsev et reported in 2021.³² After pre-treatment, BMDM in METP treatment group and DS16570511 treatment group will be further stimulated with LPS for 12 h.

Micro-CT Analysis and Histomorphometry Staining

All the joints and alveolar bone tissues were scanned and analyzed using a micro-Computed Tomography (micro-CT) system (Siemens Inveon Micro-CT, Munich, Germany). After the scanning, rebuilt images were used to perform 3D

histomorphometric analysis. For knee joint tissues, the density of subchondral bones was assessed with BV/TV, BS/BV, TbTh, TbN and TbSp parameters (Bone Surface, BS; Bone Volume, BV; Tissue Volume, TV; Trabecular Number, Tb.N; Trabecular Separation/Spacing, Tb.Sp; Trabecular Thickness, Tb.Th) to reflect trabecular bone remodeling. The alveolar bone height was measured at four different sites in two molars by recording the distance from the cemento-enamel junction (CEJ) to the top of alveolar bone crest. After the micro-CT scanning, all the tissues were treated with 17% EDTA (Proandy company, Xi'an, China) solution with gentle shaking for 4 days to 7 days at room temperature for full decalcification. Dehydrate the tissues with gradient ethanol solution and xylene, and embedded in paraffin, followed with the sagittal-oriented section at of the knee joint medial compartment and alveolar bone by microchiomer with a layer thickness of 0.3 μm . Sections were processed for hematoxylin-eosin (H&E) staining and Safranin O (Sigma-Aldrich, USA) and Fasting Green (Sigma-Aldrich, USA) and recorded images with an Olympus BX41 Microscope (Olympus, Japan). The severity of KOA is assessed by the international OARSI scoring system.³³ The articular cartilage height on KOA mouse and alveolar bone height on PD mouse were evaluated using ImageJ (ImageJ software, USA).

Immunohistochemical Staining

The paraffin sections of the medial articular cavity of KOA mice were firstly heated at 65°C for 6 h, then dewaxed with xylene and gradient alcohol solution, and boiled with sodium citrate antigen retrieval solution at high pressure for 3 minutes. After antigen retrieval, sections were treated with endogenous peroxidase eliminating agent for 10 minutes and blocked nonspecific antigen site with goat serum (Sigma-Aldrich, USA) at room temperature for 30 minutes, and then incubated with the primary antibodies for 12 h at 4°C. The primary antibodies were as follows: iNOS (D6B6S) Rabbit mab (ab15323, Abcam, UK; 1:50), Anti-TNF alpha mab (ab1793, Abcam, UK; 1:50). Then, sections were washed with PBS and incubated with goat against rabbit/mouse secondary antibodies (111–035-003 and 115–035-003, Jackson, USA; 1:200) for 1.5 h at room temperature. After PBS washing, sections were incubated with horseradish enzyme labeled streptavidin working fluid for 15 minutes, Diaminobenzidine (DAB) for 20 seconds and hematoxylin for 2 minutes in sequence (ZSGB-Bio, China). The sections were then dehydrated and sealed with neutral balsam. Recorded images of sections with an Olympus BX41 Microscope (Olympus, Japan).

Immunofluorescence Staining

Frozen sections of KOA model mouse joint with a layer thickness of 10 μm were permeabilized in 1% Triton X-100 (Sigma-Aldrich, USA) for 5 minutes, then blocked nonspecific antigen site with goat serum (Sigma-Aldrich, USA) at room temperature for 30 minutes. Incubated with Anti-F4/80 primary antibody (ab6640, Abcam, UK; 1:200) for 12 h at 4°C. Then, sections were washed and incubated with Alexa Flour 488 Goat Anti-Mouse IgG (Yeasen, Shanghai, China; 1:200) for 1.5 h at room temperature in the dark, washed and sealed with anti-fluorescence quenching mounting solution (containing 4,6-diamidino-2-phenylindole, DAPI) (P0131, Beyotime Biotechnology, Shanghai, China). Cell images were captured using the Nikon laser scanning confocal microscope (A1 Plus, Nikon, Japan). The co-localization characterized by Pearson's coefficient was evaluated using ImageJ (ImageJ software, USA).

Flow Cytometry

Prior to staining, BMDM were washed with PBS and digested by trypsin (Thermo Fisher, USA), resuspended and dispensed into 1.5mL centrifuge tubes at the density of 1×10^6 cells per 200 μL PBS. The antibodies or probes were as follows: PE Anti-CD80 mab (ab93507, Abcam, UK), PE Anti-CD86 mab (ab77226, Abcam, UK), ROS probe DCFH-DA (2,7-Dichlorodi-hydro fluorescein diacetate) (50101ES01, Yeasen, Shanghai, China), BALBcellProbe F3 for cytoplasmic calcium ($\text{c}[\text{Ca}^{2+}]$) (Baiaolaibo Technology, Beijing, China). BMDM was incubated with antibodies or probes at 37°C under dark conditions for 30 minutes, and detected and analyzed using FlowJo_v10.6.2 (FlowJo Software, USA).

Detection of Endoplasmic Reticulum (ER) or Mitochondrial Calcium Ion Levels

The ER $[\text{Ca}^{2+}]$ and m $[\text{Ca}^{2+}]$ were detected using the assay kit (GMS10153.1 v.A and GMS10267.1 v.A, GENMED company, Shanghai, China). In short, BMDM was cultured and induced on black 96 well plates. Cell sample wells,

maximum wells and blank control wells were set and processed following the manufacturer's instructions. RFU (relative fluorescence unit) was detected using the multimode plate reader (HH3400, PerkinElmer, MA, USA).

RNA Extraction, Reverse Transcription, and qPCR

Total RNA was extracted with TRIzol reagent (15-596-026, Invitrogen, USA) and converted to cDNA using PrimeScript RT Master Mix Kit (RR036A, Takara, Japan). Then, quantitative reverse transcription-polymerase chain reaction (qRT-PCR) was conducted with TB Green Premix Ex Taq II (RB820A, Takara, Japan) using the qRT-PCR System (Bio-Rad, USA). The relative expression of each gene was calculated using the $2^{-\Delta\Delta C_t}$ method for statistical analysis. The expression was normalized to the average expression of all control individuals. The housekeeping gene used was β -actin. The information on primers is shown in [Supplementary Table](#).

ELISA and Western Blotting

The concentration of cytokines in joint tissue (covering subchondral bone, cartilage, and synovial tissue between the tibia and femoral epiphysis) homogenate or the culture supernatants were measured by the enzyme-linked immuno sorbent assay (ELISA) according to the manufacturer's introductions. The joint tissue was collected as isolated right knee joint, and tissue proximal to the femoral epiphysis and distal to the tibial epiphysis were removed, leaving intact joint capsule and femoral/tibial head. For joint tissue homogenate, after sampling, the tissue was dried with absorbent paper and weighed, then radioimmunoprecipitation assay (RIPA) histiocyte lysis buffer containing protease inhibitors of 2 times the weight of tissue was added. Cut the tissue into small pieces about 1mm in diameter and digest for 20 minutes on the ice. Centrifuged at the speed of 12,000 rotations per minute and collect supernatant for later measurement. The samples of tissue homogenate or the culture supernatants were detected using ELISA Kits including TNF- α (EMC102a.96) and IL-1 β (EMC001b.96) (NeoBioscience, Wuhan, China) according to the manufacturer's instructions. The expression of actin (CW0096A, cwbiotech, China), iNOS (#13120S, Cell Signaling), Arginase-1(93668s, Cell Signaling), HIF-1 α (ab179483, Abcam) GOT1 (MA5-31526, Thermo Fisher) and NOX2 (PA5-79118, Thermo Fisher) in macrophage was measured by Western blot. Total proteins of BMDM were extracted using RIPA buffer containing protease inhibitors and assayed with Bicinchoninic Acid (BCA) protein assay reagent (Beyotime Biotechnology). Equal amounts of protein samples were loaded onto sodium dodecyl sulfate-polyacrylamide gel electrophoresis (SDS-PAGE) gels, separated by electrophoresis and later transferred to polyvinylidene fluoride (PVDF) membranes (Millipore, Germany). The membrane was blocked with 5% Bovine Serum Albumin (BSA) for 2 h at room temperature and then incubated with primary antibody at 4°C for 12 h. After a wash with PBS containing 0.1% Tween 20 (PBST), the membranes were incubated with corresponding secondary antibodies at room temperature for 2 h. Capture images with a Western-Light chemiluminescence detection system (Tanon, China). Uncropped Western blot images are shown in [Supplementary Figure 2](#).

Metabolic Analysis

Extracellular Acidification Rate (ECAR) for the glycolysis function and Oxygen Consumption Rate (OCR) for mitochondrial aerobic respiratory function were examined using the XF96 Seahorse Metabolic Analyzer (Seahorse Biosciences, North Billerica, MA). BMDM at day 7 of differentiation were plated at a seeding density of 0.8×10^5 cells/well. Prior to the metabolic test, the media was removed and replaced with Seahorse XF assay media (#102365-100) containing 25 mM glucose, 2 mM glutamine, and 20 ng/mL M-CSF and the plates containing cells were incubated for 30 min at 37°C with no CO₂. For the OCR test, 1 μ M Oligomycin was injected in port A, 1 μ M FCCP fluoro-carbonyl cyanide phenylhydrazone in port B, and 1 μ M antimycin A in port C. For the ECAR test, 56 μ L Glucose was injected in port A, 1 μ M Oligomycin in port B, and 69 μ L 2-DG in port C (All reagents from Seahorse Biosciences, North Billerica, MA). Data was collected and analyzed using wave software (Wave desktop software, Agilent Technologies, China).

Statistical Analysis

All experiments were repeated at least three times, and the data were presented as the mean \pm SD. Statistical analysis was performed by Student's *t*-test (two-tailed) with GraphPad Prism 8.0 (GraphPad Software, USA). The difference between

groups was considered statistically significant for * $p < 0.05$, ** $p < 0.01$ or *** $p < 0.001$, and the most significant for **** $p < 0.0001$. Graph analysis was performed using GraphPad Prism 8.0 (GraphPad Software, USA).

Results

Mitochondrial Ca^{2+} Levels Increase in BMDMs from KOA Mice

The KOA model was established using the modified Huith method by removing the medial meniscus and severing the anterior cruciate ligament to destabilize the unilateral right knee joint. Immediately after the operation, a positive anterior drawer test (ADT) was performed on the operative side of the knee joint, which demonstrated that the modeling operation was successful (Figure 1A). The levels of the TNF- α and IL-1 β proinflammatory cytokines in joint tissue (covering subchondral bone, cartilage and synovial tissue between the tibia and femoral epiphysis) homogenates were detected via the ELISA method. The results showed that the levels of TNF- α and IL-1 β were upregulated in the joint tissue homogenate of KOA mice compared to that of sham-operated mice ($P < 0.001$) (Figure 1B).

BMDMs were extracted from KOA and sham-operated mice, and the m[Ca^{2+}] levels in BMDMs from both groups were detected by Rhod-2-AM fluorescent probe (rhodamine 123) staining. The m[Ca^{2+}] levels in BMDMs were significantly upregulated in the KOA mice compared to the sham-operated mice (Figure 1C). To confirm the increase in macrophage number in KOA joint tissue, quantitative analysis of the F4/80 macrophage marker was performed by in situ immunofluorescence staining. Fluorescence intensity analysis showed a higher F4/80 fluorescence intensity in the OA synovial tissue than in normal synovial tissue (Figure 1D).

Intra-Articular Injection of METP NPs Alleviates Inflammation and Protects the Articular Cartilage from Structural Destruction in OA Mice

Because m[Ca^{2+}] overload was observed in OA BMDMs, METP NPs were synthesized to target cellular mitochondria and chelate local excessive calcium ions. After synthesis, the METP NPs were characterized according to morphology

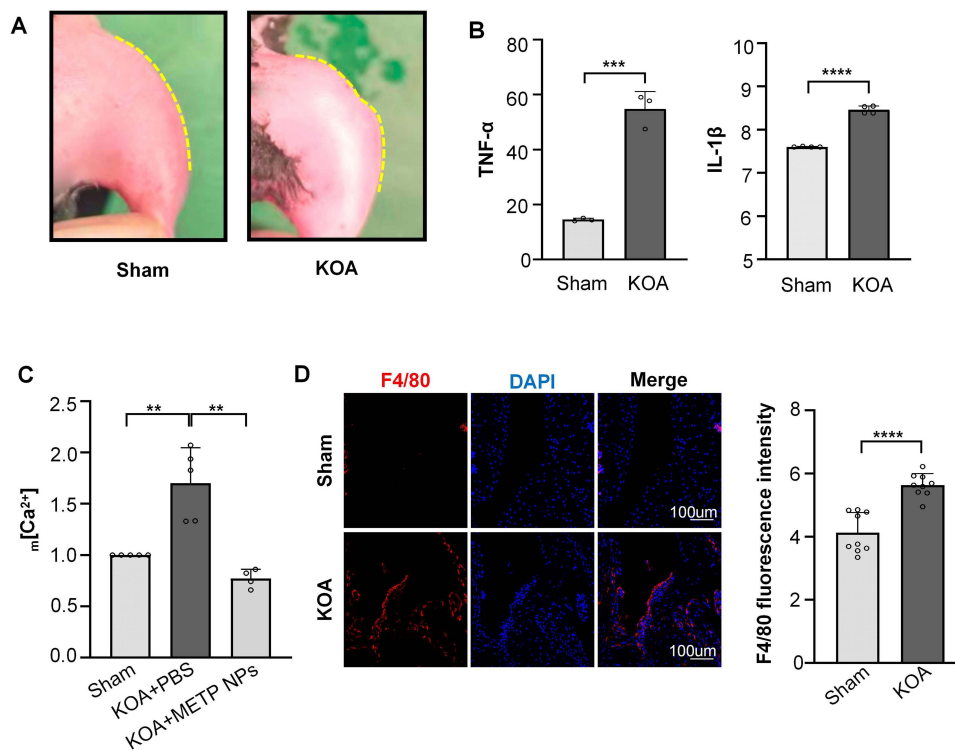


Figure 1 KOA modeling and m[Ca^{2+}] level detection in BMDMs. **(A)** Anterior drawer test (ADT) for sham and post operation KOA mice. **(B)** TNF- α and IL-1 β proinflammatory cytokine levels in joint tissue as analyzed by ELISA (pg/mL). **(C)** m[Ca^{2+}] levels in BMDMs from sham and KOA mice (fold change). **(D)** Fluorescence intensity of the F4/80 macrophage marker in joint tissue as measured by immunofluorescence staining. Yellow dotted lines mark the sagittal displacement of the tibia. Data are presented as the mean \pm SD. ** $P < 0.01$, *** $P < 0.001$ and **** $P < 0.0001$.

observed via TEM and SEM. The METP NPs were distributed as single spherical particles, ranging in size from 100 to 150 nm, after ultrasonic dispersion under a low energy level in PBS, and they were distributed as minimal aggregates with an average particle size of approximately 500 nm in powder form (Figure 2A and B). To further evaluate the particle size of METP NPs, the particle size distribution of METP NPs in PBS was detected by NTA and DLS methods. The peak METP NP size was concentrated in the range of 100 nm to 150 nm, which was consistent with the TEM results. In addition, the PDI calculated from DLS particle size data was 0.52, which confirmed that the particle size distribution of METP NPs was uniform in PBS after low-energy ultrasonic dispersion (Figure 2C and D). Moreover, the zeta potential showed that METP NPs exhibited stability in the system formed with PBS (Figure 2E). In addition, the element composition of METP NPs was analyzed by the EDS energy spectrum, and the results showed that the METP NPs were mainly composed of oxygen, carbon, silicon, phosphorus and nitrogen (Figure 2F).

To investigate the distribution of METP NPs after intra-articular injection, METP NPs were labeled with FITC fluorescent dye and then injected into the joint cavity of KOA mice. The METP NPs with green fluorescence showed a colocalization Pearson's coefficient of 0.02 with the F4/80 macrophage marker in synovial tissues of joints on the first day. With the passage of time, the proportion of colocalization between METP NPs and F4/80 fluorescence showed a progressive significant increase, reaching 0.38 at 3 days ($P < 0.01$) (Figure 1G).

To further verify the effect of METP NPs on OA mice, METP NPs and the MCU blocker, DS16570511, were injected into the joint cavity of OA mice four times as shown in the schematic (Figure 3A). The $m[Ca^{2+}]$ levels in BMDMs extracted from treated mice were detected by a Rhod-2-AM fluorescent probe. The results showed that injection of METP NPs inhibited the previously observed upregulation of BMDM $m[Ca^{2+}]$ levels in the KOA group ($P < 0.01$) (Figure 1C).

H&E and Safranin O/fast green staining was used to determine the effects of METP NP treatment in KOA mice. In the PBS treatment group, the integrity of the tibial articular was destroyed as indicated by a rough surface, decreased cartilage cell number, reduced cartilage lacuna volume and significantly lower cartilage layer thickness. At the same time, the collagen arrangement in the cartilage layer was disordered, and the tide mark was distorted and irregular in the PBS treatment group. In addition, more inflammatory cells infiltrated the subchondral bone in the PBS treatment group compared to the METP NP treatment group. For the METP treatment group, the surface morphology of the joint was relatively smooth compared to the PBS group, and the number of chondrocytes and the volume of cartilage lacunae were similar to those in the sham group. Moreover, treatment with METP NPs restored the thickness of the cartilage layer. In addition, the collagen arrangement and tide mark morphology of the cartilage layer in the METP NP treatment group were similar to those in the sham group (Figure 3B). Disease assessment using OARSI ranking showed that the PBS group and DS16570511 group had disease rankings between 2.5 and 5, while the disease ranking of the METP NP group was between 0 and 2.5 ($P < 0.0001$). The average OARSI score was 15–20 points in the PBS injection group, which was higher than in the sham group (0 points) and METP NP treatment group (0–5 points), while the score in the DS16570511 treatment group was only slightly lower than that in the PBS injection group ($P < 0.0001$) (Figure 3C). However, analysis of tibial subchondral bone by microCT in each group showed that there was no significant difference in bone parameters, including BV/TV, BS/BV, TbTh, TbN and TbSp (Supplementary Figure 3A and B).

We next performed in situ immunohistochemical staining of knee joint tissue sections to observe the levels of TNF- α and inducible nitric oxide synthase (iNOS) among the four groups. The number of TNF- α - and iNOS-positive pigmented cells in the PBS injection group and DS16570511 treatment group was increased compared to the sham group, but there were fewer TNF- α - and iNOS-positive pigmented cells in METP NP group (Figure 3D).

The pathological results showed that local injection of METP NPs had no significant effect on the tissue structure of the mouse heart, liver, spleen, lung or kidney (Supplementary Figure 3C).

METP NPs Regulate Calcium Homeostasis in BMDMs Under LPS Stimulation in vitro

To clarify the effects of METP NPs on $m[Ca^{2+}]$ levels and global calcium homeostasis in macrophages under an inflammatory microenvironment, changes in the $m[Ca^{2+}]$ level, ER $[Ca^{2+}]$ level and c $[Ca^{2+}]$ level in LPS-activated macrophages were investigated. Firstly, to explore whether macrophages actively capture and internalize METP NPs in vitro, METP NPs were conjugated with a FITC fluorescent dye and incubated with BMDMs. Mitochondria were

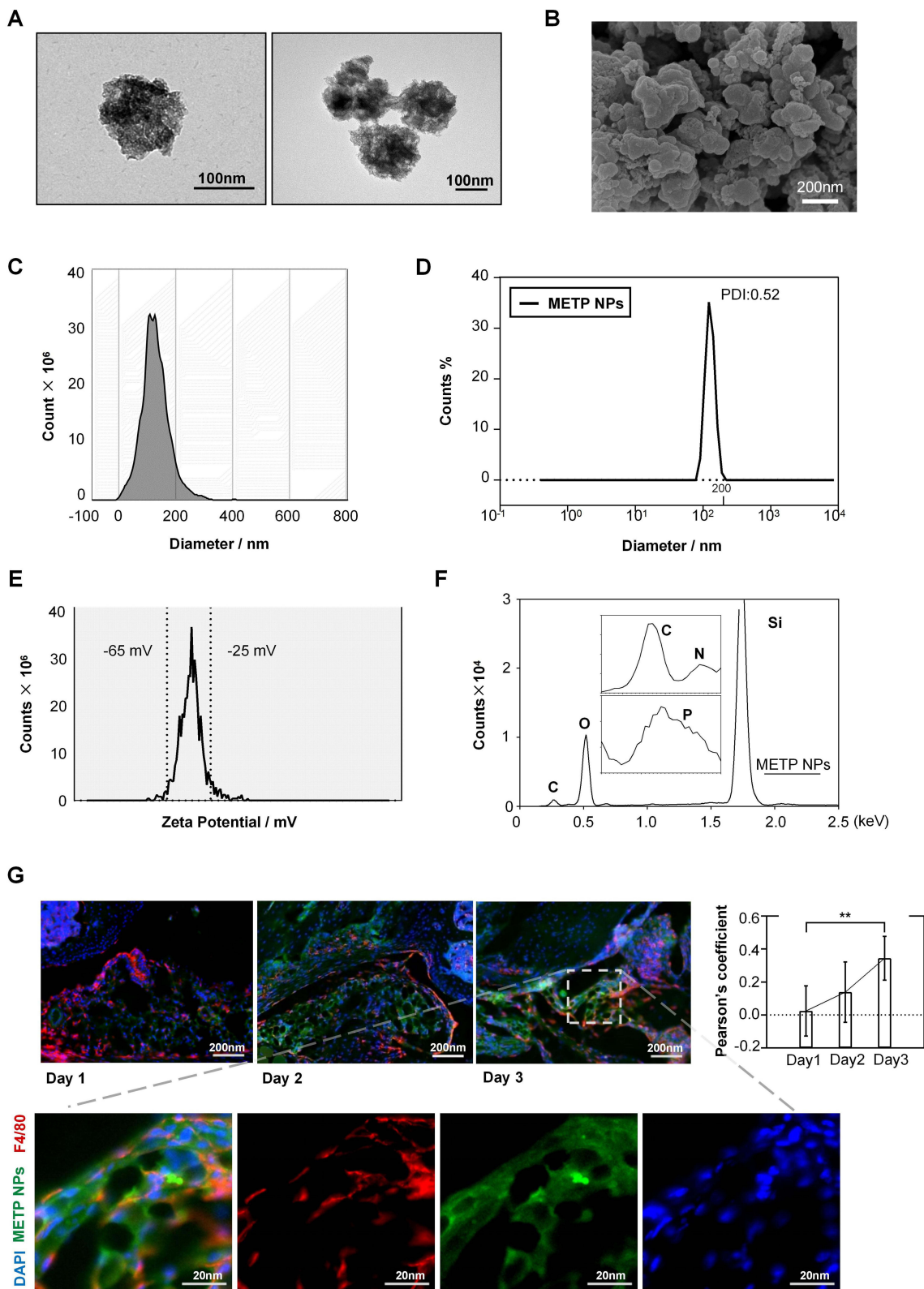


Figure 2 Characterization and in vivo colocalization of METP NPs. NPs were characterized (**A and B**) by TEM and SEM imaging of the particle size and morphology of METP NPs in PBS and in powder form, respectively. (**C**) Particle size analysis by NTA. (**D**) Particle size, polydispersity and PDI index analyses by DLS. (**E**) Zeta potential analysis. (**F**) Energy spectrum according to EDS describing the composition of elements in METP NPs. (**G**) Immunofluorescence colocalization images of macrophages (red) and METP NPs (green) in joint tissue sampled on Days 1, 2 and 3 after intracellular injection. Cell nuclei are labeled with DAPI. keV, kilo electron volt; C, N, O, Si and P for carbon, nitrogen, oxygen, silicon and phosphorus respectively. Data are presented as the mean \pm SD. **P < 0.01.

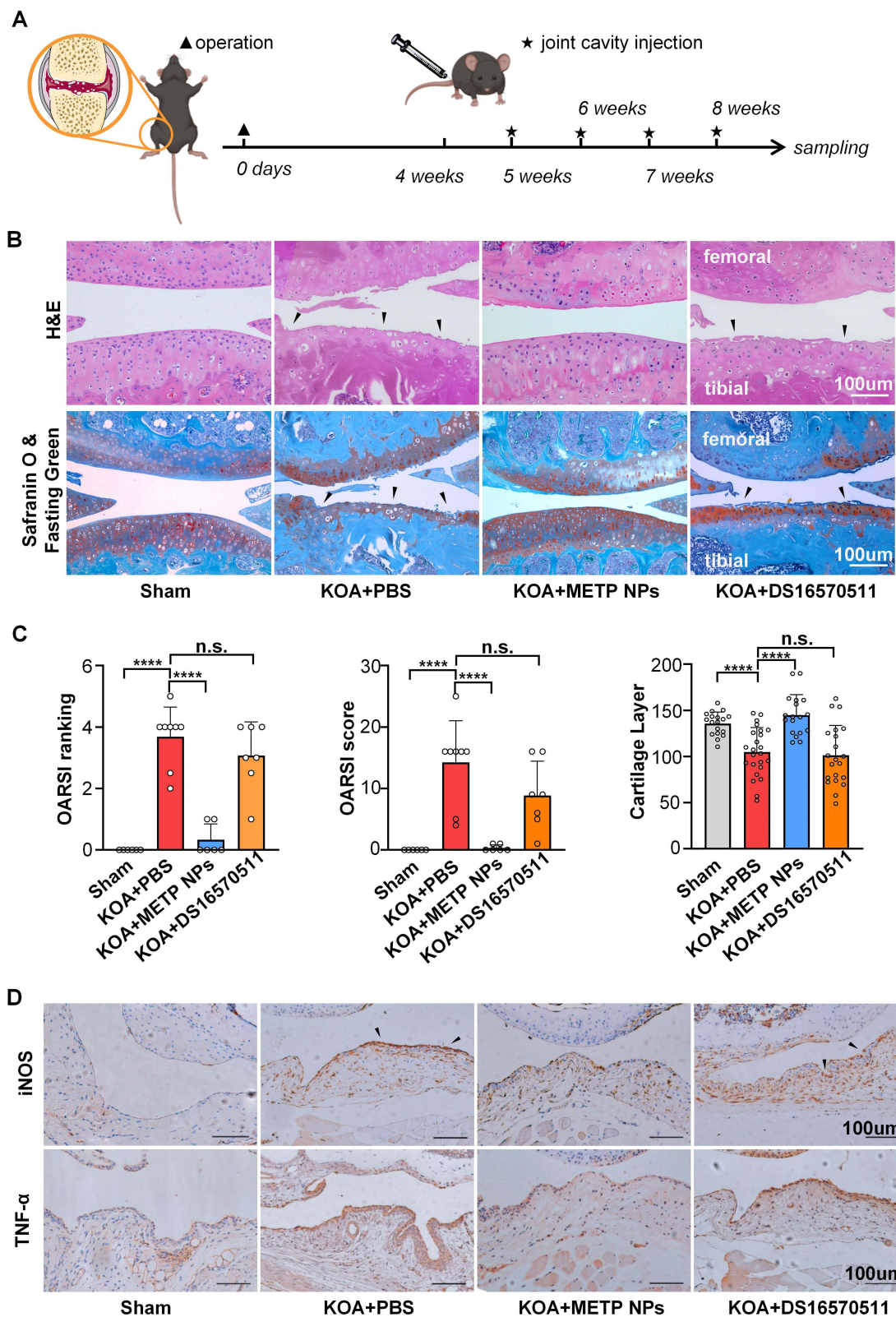


Figure 3 Intra-articular injection of METP NPs alleviates inflammation and protects articular cartilage from structural destruction in KOA mice. **(A)** Schematic graph for time points of KOA operation and injection. **(B)** The morphology of mouse joint tissue was assessed by H&E and Safranin O/fast green staining. **(C)** OARSI ranking, OARSI score and cartilage layer thickness measurement. **(D)** Immunohistochemistry staining of the iNOS and TNF- α levels in the synovium of mice in all four groups. Black triangular arrows indicate articular cartilage defect in **(A)** and strong positive reacted cells and regions in **(D)**. Data are presented as the mean \pm SD. **** $P < 0.0001$. **Abbreviation:** n.s., not significant.

specifically labeled with the MitoTracker Deep Red probe at each time point. The infrared and green fluorescence signals were analyzed by Pearson's coefficient index and statistically analyzed. The colocalization of infrared and FITC fluorescence signals increased and reached a peak within 24–48 h ($P < 0.05$) but decreased at 72 h ($P < 0.0001$), which indicated that the METP NPs were internalized by macrophages at 24–48 h and targeted to mitochondria (Figure 4A and B).

Secondly, to further explore the effect of different concentrations of METP NPs on regulating $m[Ca^{2+}]$ levels in proinflammatory macrophages, BMDMs were treated with a concentration gradient of METP NPs from 0 to 100 $\mu\text{g/mL}$ for 24 h followed by LPS stimulation for 12 h. Measurement of $m[Ca^{2+}]$ levels indicated that LPS stimulation induced a significant increase in $m[Ca^{2+}]$ levels in BMDMs in vitro ($P < 0.01$), reaching an average of 33 nM, whereas treatment with 1, 10 and 50 $\mu\text{g/mL}$ METP NPs gradually decreased the $m[Ca^{2+}]$ levels in BMDMs. In the METP NP treatment group at a concentration of 50 $\mu\text{g/mL}$, the $m[Ca^{2+}]$ levels decreased to 25 nM compared to 33 nM in the LPS alone group, which was the closest to that in the NC group (20 nM) among all the treatment groups ($P < 0.05$) (Figure 4C).

In addition to the $m[Ca^{2+}]$ levels, the $c[Ca^{2+}]$ and $ER[Ca^{2+}]$ levels in BMDMs were also detected to clarify the overall effect of METP NPs on calcium ion homeostasis in the different functional regions of the cell. The $ER[Ca^{2+}]$ and $c[Ca^{2+}]$ levels were labeled with a Mag-Flou-AM ER calcium-specific fluorescent probe and a F03 calcium probe, respectively. The $ER[Ca^{2+}]$ level was significantly decreased in the LPS treatment group compared to the NC group ($P < 0.001$), but there was no significant difference in the $ER[Ca^{2+}]$ levels between the NC group and METP NP treatment group (Figure 4D). There were no significant differences in the $c[Ca^{2+}]$ levels among the NC group, METP NP treatment group and LPS stimulation group. However, the $c[Ca^{2+}]$ level was significantly upregulated in the DS16570511 treatment group compared to the other three experimental groups ($P < 0.0001$) (Figure 4E).

To explore the cytotoxicity of METP NPs, the apoptosis of BMDMs before and after METP NP treatment was observed using Annexin-V and 7-AAD dyes to label early apoptotic cells and late apoptotic cells, respectively. Flow cytometry analysis showed no significant change in the proportion of Annexin-V⁺ 7-AAD⁻ single-positive BMDMs and Annexin-V⁺ 7-AAD⁺ double-positive BMDMs before and after METP NP treatment (Supplementary Figure 4A).

METP NPs Reduce the Proinflammatory Phenotype of BMDMs Under LPS Stimulation in vitro

After determining the effects of METP NPs on global calcium homeostasis in BMDMs, we investigated the effects of METP NPs on the BMDM proinflammatory phenotype by detecting the phenotype changes using various methods. Firstly, flow cytometry analysis showed that the expression of CD80 ($P < 0.0001$) and CD86 ($P < 0.01$) was significantly upregulated in the LPS stimulation group as assessed by the mean fluorescence intensity. The expression of CD80 in the METP NP treatment group was significantly lower than that in the LPS stimulation group ($P < 0.001$), but the expression of CD86 in BMDMs was not significantly differentiate among the LPS stimulation, METP NP treatment and DS16570511 treatment groups (Figure 5A).

To evaluate the cytokine secretion level of BMDMs, the concentrations of the TNF- α and IL-1 β proinflammatory cytokines in the culture supernatant were detected. The levels of secreted TNF- α were significantly increased in the LPS stimulation group ($P < 0.01$) but decreased in the METP NP treatment group ($P < 0.05$). However, there was no significant difference in the TNF- α secretion level between the DS16570511 treatment and LPS stimulation group. The levels of secreted IL-1 β were similar to those of secreted TNF- α . After LPS stimulation, the secretion level of IL-1 β was significantly increased ($P < 0.0001$), but the secretion levels of IL-1 β in the METP NP treatment group ($P < 0.0001$) and DS16570511 treatment group ($P < 0.001$) decreased (Figure 5B). In addition to the surface markers and cytokine secretion levels, the protein expression levels of inducible nitric oxide synthase (iNOS) and arginase 1 (ARG1) in BMDMs were detected by Western blot analysis. The expression level of iNOS was significantly increased after LPS stimulation ($P < 0.01$) but significantly decreased after treatment with METP NPs or DS16570511 ($P < 0.05$), while no statistical difference in iNOS expression level was observed between the METP NP and DS16570511 treatment groups. In addition, there were no significant differences in the expression levels of the ARG1 anti-inflammatory marker among the four groups (Figure 5C and D).

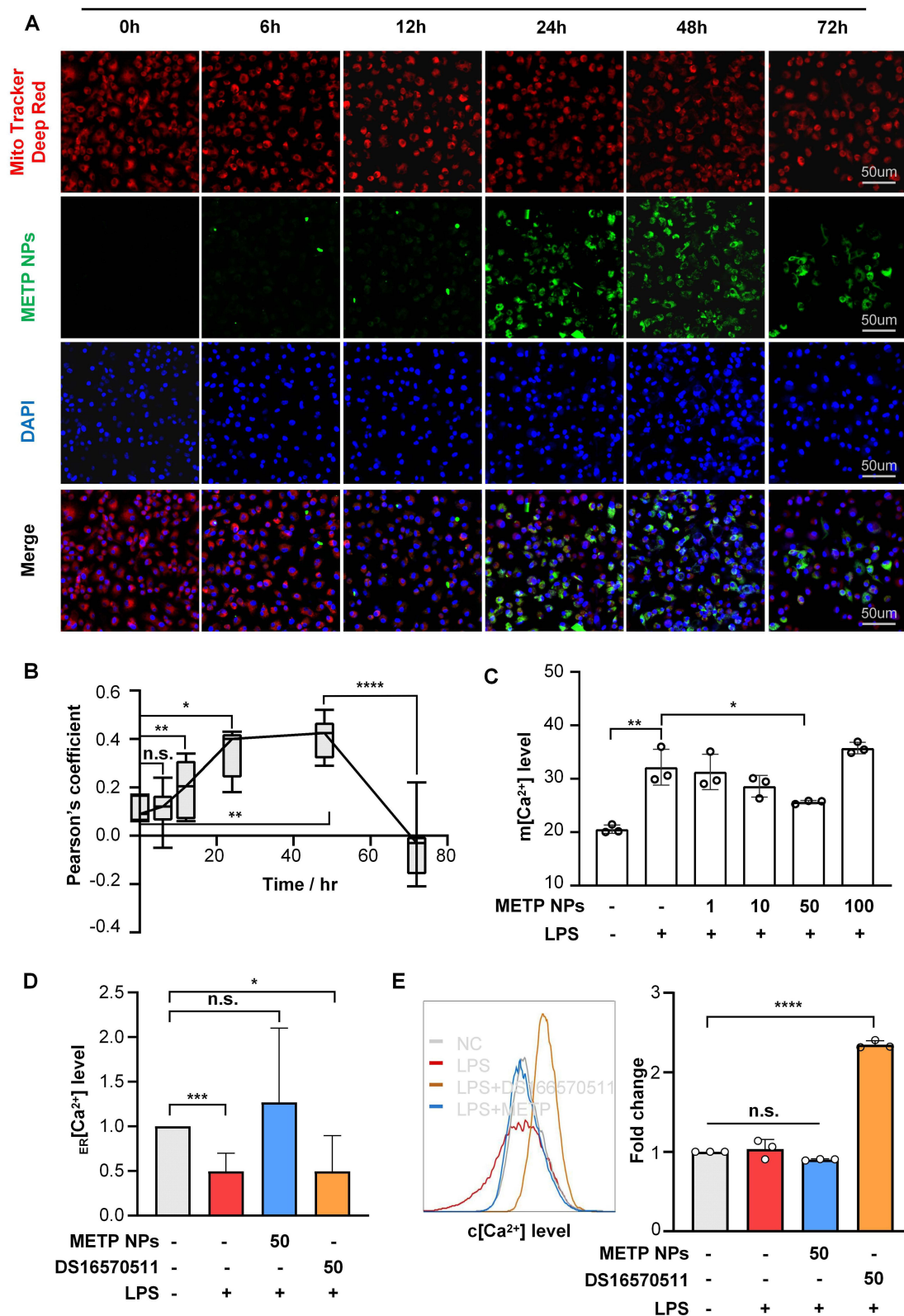


Figure 4 METP NPs regulate calcium homeostasis in BMDMs under LPS stimulation in vitro. **(A)** Immunofluorescence staining showing colocalization of FITC-labeled METP NPs with the MitoTracker Deep Red probe at different treatment periods. **(B)** Colocalization analysis with Pearson's coefficient (ranging -1 to 0, negative correlation; ranging 0 to 1, positive correlation). **(C)** m[Ca²⁺] levels in BMDMs under LPS stimulation pretreated with a gradient concentration of METP NPs. Flow cytometry analysis of **(D)** ER[Ca²⁺] level and **(E)** c[Ca²⁺] level for all four groups. The concentration of METP NPs is shown in µg/mL, and the concentration of DS16570511 is shown in µM. Data are presented as the mean ± SD. *P < 0.05, **P < 0.01, ***P < 0.001 and ****P < 0.0001.

Abbreviation: n.s., not significant.

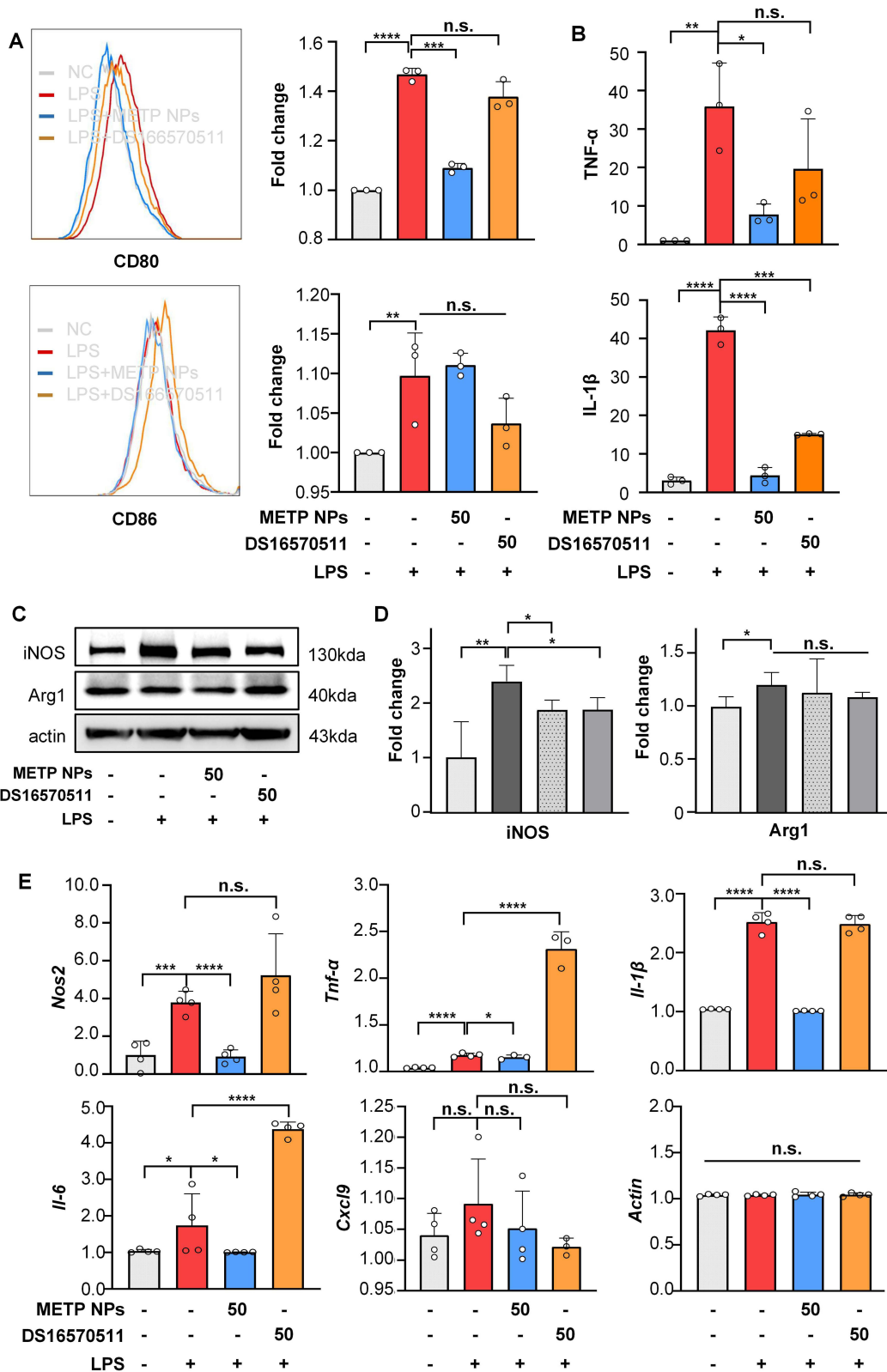


Figure 5 METP NPs reverse the proinflammatory phenotype in BMDMs under LPS stimulation in vitro. **(A)** Expression levels of the CD80 and CD86 macrophage surface markers according to flow cytometry analysis. **(B)** Secretion levels of the TNF- α and IL-1 β proinflammatory cytokines according to ELISA (pg/mL). **(C and D)** Protein expression level of the iNOS and ARG1 macrophage markers according to Western blot analysis. **(E)** The gene transcription levels of Nos2, TNF- α , IL-1 β , IL-6, Cxcl9 and actin were detected by qRT-PCR in all four groups. The concentration of MET NPs is shown in μ g/mL, and the concentration of DS16570511 is shown in μ M. Data are presented as the mean \pm SD. *P < 0.05, **P < 0.01, ***P < 0.001 and ****P < 0.0001.

Abbreviation: n.s., not significant.

The expression of proinflammatory genes in BMDMs was detected via qRT-PCR. The mRNA levels of Nos2, TNF- α , IL-1 and IL-6 were significantly increased in the LPS stimulation group compared to the NC group ($P < 0.05$) but were significantly decreased in the METP NP group ($P < 0.05$). Compared to the LPS stimulation group, these proinflammatory genes were not significantly reduced in the DS16570511 treatment group, and the levels of TNF- α and IL-6 were higher in the DS16570511 treatment group ($P < 0.0001$) (Figure 5E).

METP NPs Inhibit the Proinflammatory Mitochondrial Metabolic Characteristics of BMDMs Stimulated by LPS in vitro

To explore how $m[Ca^{2+}]$ affects the BMDM proinflammatory phenotype, the energy metabolism types and characteristic metabolite levels of BMDMs treated with METP NPs or DS16570511 under LPS stimulation were detected in vitro based on mitochondrial metabolism. Firstly, the oxidative phosphorylation and glycolysis levels of BMDMs were measured by a Seahorse cell energy analyzer. At 12 h after LPS stimulation, the overall ECAR level of BMDMs was significantly higher compared to the NC group, but there was no significant change in the OCR basal level among all the groups (Figure 6A). However, in the METP NP treatment group and DS16570511 treatment group, BMDMs showed limited maximal respiration and spare capacity compared to the NC group and LPS stimulation group ($P < 0.05$) (Figure 6B). Compared to the LPS stimulation group, the METP NP and DS16570511 treatment group showed decreased baseline glycolysis and glycolysis capacity, and the decreases were more significant in the METP NP group than in the DS16570511 treatment group ($P < 0.05$) (Figure 6B).

To measure cellular oxidative stress levels, which are closely related to $m[Ca^{2+}]$ overload, ROS were labeled and detected with 2, 7-dichloride-hydro fluorescein diacetate (DCFH-DA) dye in all the groups. Compared to the NC group, the intracellular ROS levels in the LPS stimulation group were significantly higher ($P < 0.01$), and this upregulation was suppressed in the METP NP treatment group ($P < 0.05$). However, after treatment with the MCU blocker (DS16570511), the ROS levels in BMDMs were significantly upregulated and higher than those in the NC group ($P < 0.05$) (Supplementary Figure 4B). Western blot analysis for nicotinamide adenine dinucleotide phosphate oxidase 2 (NOX2) showed that the protein expression levels of NOX2 were not significantly different among the NC group, LPS stimulation group and METP NP treatment group but were significantly increased in the DS16570511 treatment group compared to the other groups ($P < 0.05$) (Supplementary Figure 4C and D).

To further explore the effect of METP NPs on the expression of proinflammatory metabolites in LPS-stimulated BMDMs, Western blot analysis was used to detect the expression levels of HIF-1 α and the cytosolic aspartate aminotransaminase, glutamic-oxaloacetic transaminase 1 (GOT1). The expression levels of HIF-1 α ($P < 0.05$) and GOT1 ($P < 0.01$) were significantly increased in the LPS stimulation group. Compared to the LPS stimulation group, the levels of HIF-1 α and GOT1 were significantly decreased after METP NP treatment ($P < 0.05$) (Figure 6C and D).

We next examined the differences in pyruvate utilization and the expression of proinflammatory metabolic characteristic products among the four groups. Firstly, to elucidate the changes in pyruvate supply and consumption in macrophages, the concentrations of pyruvate in the BMDMs and culture supernatant were measured using a colorimetric method. In the LPS stimulation group, the cytoplasmic pyruvate concentration was significantly increased in the BMDMs, while the pyruvate concentration in the culture supernatant was significantly decreased ($P < 0.01$). Compared to the NC group, the cytoplasmic pyruvate concentrations in the METP NP and DS16570511 treatment groups were not statistically different, and the pyruvate concentration in the cell culture supernatant was higher in the METP NP treatment group and DS16570511 treatment group compared to the LPS stimulation group. In addition, the decrease in the pyruvate concentration in the cell culture supernatant was more subtle in the METP NP treatment group than in the DS16570511 treatment group ($P < 0.01$) (Figure 6E).

To explore the general therapeutic effect of METP NPs on chronic inflammation involving macrophages, a PD mouse model was established to evaluate the anti-inflammatory effect of METP NPs. To explore the differences in the level of alveolar bone loss (ABL) among groups, microCT was used to detect the level of ABL at the first maxillary molars of mice. The results showed that the level of ABL at the mesiobuccal root of the first molars of PD mice was significantly higher than that in the sham group, and the ABL level in METP NP-treated mice was significantly lower than that in the

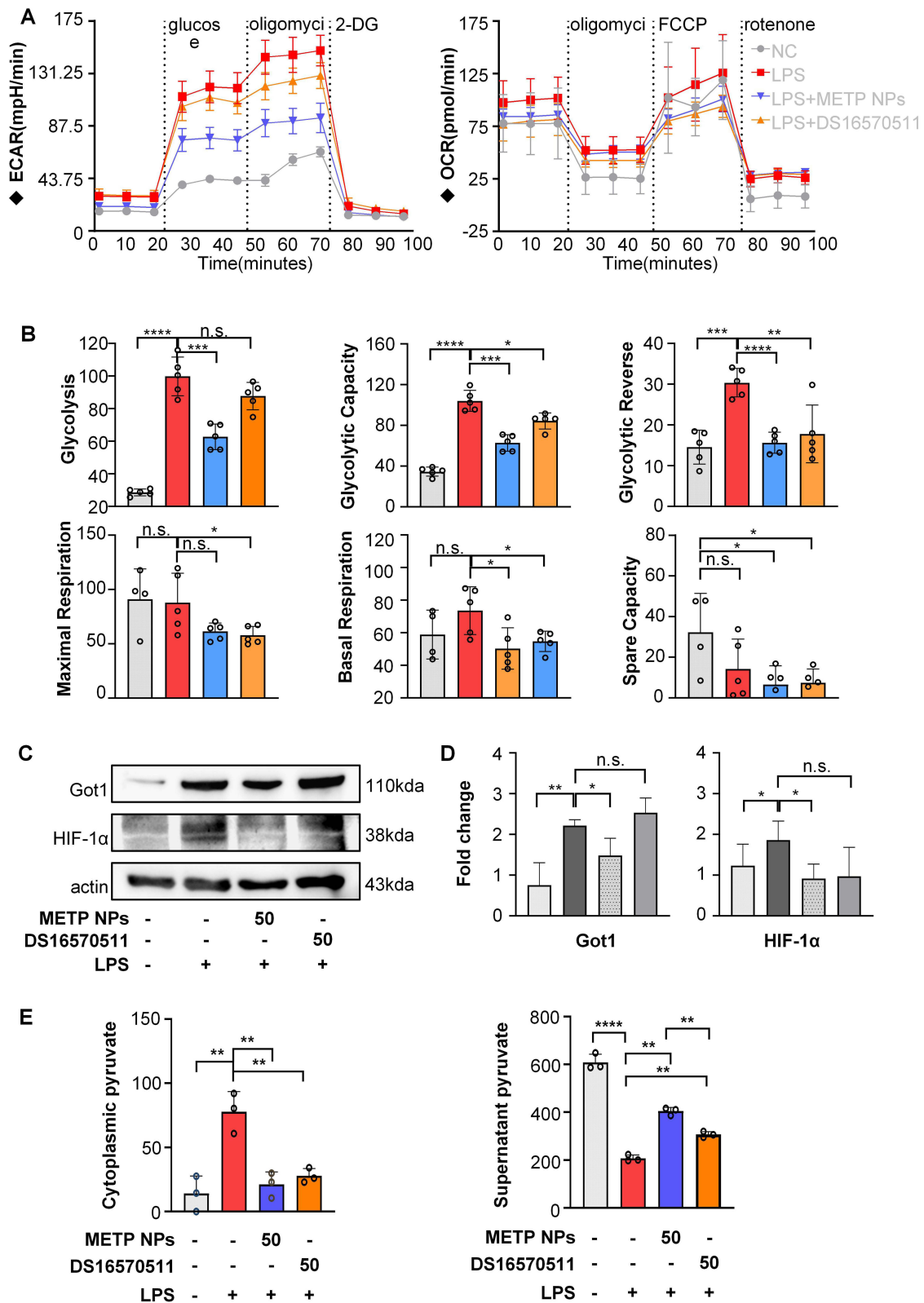


Figure 6 METP NPs inhibit the proinflammatory mitochondrial metabolic characteristics of BMDMs stimulated by LPS. **(A)** ECAR and mitochondrial respiration OCR level as measured by a Seahorse cell energy analyzer. **(B)** Glycolysis, glycolytic capacity and glycolytic reserve were calculated from ECAR, and maximal respiration, basal respiration and spare capacity were calculated from OCR. **(C and D)** Protein expression level of the aspartate-arginosuccinate shunt key enzyme, GOT1, and the characteristic product, HIF-1 α , by Western blot analysis. **(E)** Cytoplasmic and supernatant pyruvate levels of all four groups. The concentration of METP NPs is shown in $\mu\text{g}/\text{mL}$, and the concentration of DS16570511 is shown in μM . The ECAR-related parameters are shown in mpH/min, and the OCR-related parameters are shown in pmol/min. Data are presented as the mean \pm SD. * $P < 0.05$, ** $P < 0.01$, *** $P < 0.001$ and **** $P < 0.0001$.

Abbreviation: n.s., not significant.

PD mice. However, no significant difference in ABL level was observed between the DS16570511-treated mice and the PD mice ([Supplementary Figure 5A](#) and [B](#)). The alveolar bone height in the periodontal tissue was evaluated by H&E staining ([Supplementary Figure 5C](#)), which demonstrated a significant recovery of alveolar bone height in METP NP-treated mice compared to PD mice, but this recovery was not observed in DS16570511-treated mice.

Discussion

OA is characterized by chronic inflammation and structural destruction of joints. As mentioned earlier, macrophages in OA tissues migrate to the lesion site where they are enriched and transform towards the proinflammatory phenotype. Persistent proinflammatory macrophages are associated with the failure of healing of chronic skin wounds, myocardial infarction and OA.^{34–36} Therefore, the continuous enrichment of proinflammatory macrophages is a potential therapeutic target of chronic inflammatory diseases, such as OA. However, drugs that target $m[Ca^{2+}]$ influx to inhibit $m[Ca^{2+}]$ overload and related macrophage proinflammatory phenotypes still have many shortcomings.

In the present study, we designed and synthesized METP NPs, which were characterized by TEM, SEM, DLS, NTA and EDS. Functional experiments confirmed that METP NPs specifically trapped calcium ions in both calcium-only solutions and mixed solutions containing Ca^{2+} , Mg^{2+} , Na^+ and K^+ .³⁷ Our previous study demonstrated that the precision engineered METP/si β -catenin NPs have a considerable therapeutic effect on OA mice by targeting mesenchymal stem cells (MSCs) located in subchondral bone by blocking the osteogenic detrimental Wnt/ β -catenin pathway with preloaded siRNA and restoring the mitochondrial function of MSCs.³⁷ However, due to the persistence of abnormal mechanical forces on the cartilage, MSC-mediated cartilage regeneration is difficult to achieve to some extent. The application of NPs in OA to alleviate inflammation to trigger endogenous regeneration may be another alternative. We unexpectedly found that the intermediate product of METP/si β -catenin NP synthesis, METP NP without siRNA, also had a therapeutic effect on cartilage height recovery in OA mice by subchondral bone injection.³⁷ However, it remained unknown whether and how METP NPs target macrophages in the joint cavity to relieve the tissue inflammation in OA.

In the present study, we demonstrated the therapeutic effect of METP NPs in KOA mice through intra-articular injection. Given that intra-articular injection is more common and convenient for both clinical and experimental OA administration,^{38,39} we shifted the injection site accordingly and injected METP NPs into the joint cavity of OA mice to investigate tissue inflammatory recovery. According to the study by Lizette et al, on the 28th day after the establishment of the KOA model, the number of macrophages in the joint tissue does not increase, and they are not activated; however, during the period from 28 to 56 days, the number of macrophages in the joint tissue gradually increase, and the proportion of proinflammatory macrophages is increased.⁴⁰ Based on this previous study, we selected 4 weeks after the KOA modeling operation as the time point for intra-articular injection in the present study. We confirmed that METP NPs effectively ameliorated the destruction of OA joint structure, and METP NP injection significantly reduced OA inflammation with a corresponding significant reduction in the levels of tissue inflammatory cytokines ([Figure 3](#)). In addition, there was no obvious difference in OA articular cartilage bone trabeculae diameter, bone trabeculae density or bone cortex thickness among the four groups according to the analysis of the indicators. Because the subchondral bone destruction and reconstruction in OA is a long-term process, the subchondral bone may not have been significantly changed at 8 weeks, which agreed with the conclusion of Lin et al.⁴¹

To explore how METP NPs play a role in the treatment of OA, we performed localization tracking and functional analysis after injecting METP NPs into the articular cavity of OA mice. Considering that macrophages are mainly responsible for the capture and clearance of exogenous non-physiological foreign bodies, such as MSN silica particles,^{27–30} we hypothesized that macrophages may effectively internalize METP NPs after application in vivo, which was confirmed with a fluorescence colocalization experiment. By detecting the iNOS macrophage proinflammatory marker, we confirmed that METP NPs inhibited the proinflammatory phenotype of synovial macrophages. We next examined the $m[Ca^{2+}]$ levels in macrophages in OA. Because the absolute number of macrophages in the joint cavity and synovium in situ was small and difficult to obtain, we extracted BMDMs from OA mice given OA is a total joint disease, including bone marrow lesions.^{42,43} The results indicated that the $m[Ca^{2+}]$ levels in BMDMs of OA mice were upregulated and that METP NPs reduced the $m[Ca^{2+}]$ levels in BMDMs to a relatively normal level. Thus, the efficacy of METP NP treatment as an $m[Ca^{2+}]$ influx inhibitor was demonstrated by the therapeutic outcome of OA.

Mitochondria are not only organelles for biosynthesis and energy supply but are also important signal transduction sites in cells. Calcium homeostasis, which is important in cell survival and function, requires fine-tuned release and uptake of calcium via calcium-related proteins and channels. The $c[Ca^{2+}]$, $m[Ca^{2+}]$ and $ER[Ca^{2+}]$ levels constitute the homeostasis of cellular calcium. As an important component of intracellular calcium homeostasis, the $m[Ca^{2+}]$ level is influenced by the $ER[Ca^{2+}]$ level and $c[Ca^{2+}]$ level, and vice versa.^{44–46} To explore the effect of $m[Ca^{2+}]$ level intervention on intracellular calcium homeostasis, we first selected the optimum conditions of METP NPs applied to BMDMs *in vitro* through the colocalization experiment with a time gradient from 0 to 72 h to clarify the time-dependent process by which METP NPs are internalized by BMDM and targeted to mitochondria. Based on these experiments, we selected 24–48 h as the administration time period. Secondly, we established a concentration gradient of METP NPs and selected 50 $\mu\text{g}/\text{mL}$ as the optimal concentration to regulate the $m[Ca^{2+}]$ level of BMDMs. In addition, we also examined the effect of METP NPs on the $ER[Ca^{2+}]$ level in BMDMs. The ER is an important calcium ion storage, which can be activated by both electrical and chemical stimulation, and it modulates calcium ion flux. In response to stimulation, ER calcium is released from the high-concentration lumen, resulting in a sharp increase in cytoplasm calcium concentration (approximately 10 μM).⁴⁴ LPS-treated BMDMs showed a significant decrease in the $ER[Ca^{2+}]$ levels, which may be related to the continuous activation of the $ER[Ca^{2+}]$ release pathway under inflammatory stimulation, while the $ER[Ca^{2+}]$ levels in BMDMs pretreated with METP NPs were not significantly different from NC BMDMs, suggesting a decrease in ER calcium release. Finally, we measured the changes in the $c[Ca^{2+}]$ levels in BMDMs in each group. The $c[Ca^{2+}]$ level is usually stable (approximately 100 nM)⁴⁵ and is much lower than that in the ER lumen, which may reach 100 μM under rest conditions and 0.5 mM under stimulation.⁴⁶ The increase of $c[Ca^{2+}]$ in macrophages is detrimental to inflammation resolution and tissue repair. Calcium uptake through MCU can buffer $c[Ca^{2+}]$ disturbance, and $c[Ca^{2+}]$ increase induces activation of the MEK kinase 1 (MEKK1) inhibitory nuclear factor kappa B (NF- κ B) kinase, which promotes iNOS and TNF- α production.²¹ Previous studies have shown that the transition of macrophages to a proinflammatory phenotype requires the influx of extracellular calcium,⁴⁷ and the reduction of $c[Ca^{2+}]$ promotes the anti-inflammatory phenotype.⁴⁸ In the present study, LPS treatment had no significant effect on $c[Ca^{2+}]$, while BMDMs pretreated with the MCU blocker, DS16570511, showed a significant increase in $c[Ca^{2+}]$ levels, which may be due to DS16570511 blocking the uptake of ER-derived calcium flow into the mitochondrial lumen. The accumulation of calcium ions in the cytoplasm induces proinflammatory activation of BMDMs, which was consistent with our research on the activation of the BMDM phenotype.

We next verified that METP NPs inhibited the proinflammatory activation of macrophages *in vitro* by measuring BMDM surface markers, gene transcription, protein expression and cytokine secretion levels. The MCU blocker, DS16570511, had a lesser effect on inhibiting proinflammatory activation of macrophages than METP NPs as the METP NPs regulated the depletion of locally excess calcium ions by chelation in the BMDMs but not by blocking the flow of normal calcium ions between organelles. These findings suggested that METP NPs have advantages as $m[Ca^{2+}]$ regulators as they had a minimal effect on overall intracellular calcium homeostasis compared to the small molecule MCU blocker.

It remains unclear how METP NP modulation of $m[Ca^{2+}]$ subsequently affects the macrophage phenotype. As an important organelle of energy metabolism in cells, mitochondrial metabolism is one of the most important downstream pathways regulated by $m[Ca^{2+}]$. In macrophages, different types of metabolites significantly affect phenotypic differentiation. Existing evidence suggests that $m[Ca^{2+}]$ induces proinflammatory metabolism in macrophages. Compared to resting macrophages, proinflammatory macrophages are characterized by Warburg metabolism¹⁶ with enhanced glycolysis, maximal glycolysis capacity, and disrupted metabolism of tricarboxylic acid (TCA) cycle carbon flow, showing higher levels of citrate, itaconate and succinate.⁴⁹

We next detected the overall OCR and ECAR levels of LPS-stimulated BMDMs pretreated with METP NPs and found that the metabolic characteristics of LPS-stimulated BMDMs mainly comprised a significant upregulation of glycolysis, which was consistent with the published findings described above. However, inhibition of LPS-induced $m[Ca^{2+}]$ elevation with METP NPs resulted in the inhibition of glycolytic levels and glycolytic reserves in BMDMs. In addition, succinic acid in the Krebs cycle promotes the stabilization of HIF-1 α in proinflammatory macrophages via the aspartate-arginosuccinate shunt, thereby driving the sustained production of proinflammatory and glycolytic genes.^{14,16} In the present study, the expression of the aspartate-arginosuccinate shunt rate-limiting enzyme, GOT1, which is characteristic of proinflammatory metabolism, also decreased after METP NP pretreatment along with a decrease in

the HIF-1 α proinflammatory factor. The resting level of OCR in the BMDMs did not change after LPS stimulation, but BMDMs pretreated with METP NPs showed inhibited oxidative phosphorylation. In addition, METP NPs inhibited LPS-induced ROS production in BMDMs. Taking into account the OCR results above, BMDMs pretreated with METP NPs showed a limited oxidative phosphorylation process, indicating that the inhibited oxidative phosphorylation of BMDMs may be related to the ROS generation process under the inhibition of m[Ca²⁺] signaling, which was consistent with the phenomenon observed by Seegren et al.⁵⁰ These findings suggested that the downstream mechanism of METP NPs regulating m[Ca²⁺] to inhibit the proinflammatory phenotype of BMDMs may occur via inhibiting the proinflammatory aspartate-arginosuccinate shunt and m[Ca²⁺]-related generation of ROS in macrophages.

Pyruvate, the end product of glycolysis, is located at an important intersection of cellular metabolic networks. m[Ca²⁺] signaling reprograms mitochondrial metabolism by enhancing pyruvate supply to meet the bioenergy requirements and generate ROS.⁵⁰ Consistently, we detected and observed significantly lower pyruvate uptake and utilization levels in LPS-stimulated BMDMs pretreated with METP NPs compared to NC BMDMs. In addition to inducing proinflammatory metabolic characteristics and ROS generation, m[Ca²⁺] also affects the macrophage phenotype in other ways, such as affecting c[Ca²⁺] concentration.^{20,21} As mentioned above, METP NPs regulated the level of m[Ca²⁺] without affecting the level of c[Ca²⁺], suggesting that METP NPs are superior to the small molecule MCU blocker in regulating m[Ca²⁺].

To further verify the control effect of METP NPs on chronic inflammation, we utilized another PD model. PD is a chronic inflammatory disease dominated by plaques composed of a variety of bacteria and involves the immune system, resulting in progressive resorption of alveolar bone and loss of periodontal attachment.⁵¹ We induced periodontal tissue inflammation and alveolar bone resorption by local injection of LPS and set up sham, PD, PD+METP NP and PD+DS16570511 groups consistent with the KOA model. The results showed that METP NPs effectively protected alveolar bone from resorption induced by LPS stimulation, and treatment with METP NPs had better recovery effects on alveolar bone height than DS16570511 administration. The experimental results of METP NP treatment for PD will help to develop new strategies for METP NP treatment.

As a simplified form of METP/si β -catenin NPs, METP NPs have a simpler chemical structure, making the synthesis process shorter and easier to obtain. In addition, METP NPs do not contain bioactive siRNA. The present study demonstrated that the administration of METP NPs via intra-articular injection achieved desirable efficacy in the treatment of OA in mice by inhibiting the macrophage-induced inflammatory response in the early stage of the lesion. Compared to METP/si β -catenin NPs, METP NPs showed additional advantages in terms of biological safety and economic effects, which will help further promote METP NPs to the clinical application stage.

Conclusion

In conclusion, we demonstrated that METP NPs inhibited calcium ion influx in macrophage mitochondria with advantageous regulatory effects and target accuracy. Based on the macrophage uptake of METP NPs with pretreatment or injection into the joint cavity, we demonstrated that METP NPs reversed the increase of calcium ions in mitochondria of activated BMDMs, thus inhibiting the proinflammatory phenotype of BMDMs by suppressing the proinflammatory-related metabolism. Furthermore, METP NPs regulated the phenotype of macrophages *in vivo*, which blocked the OA inflammatory cascades at an early stage and controlled the OA-induced structure destruction, thereby achieving a considerable therapeutic effect in alleviating OA in mice. The present study provided new therapeutic strategies for METP NPs application in chronic inflammatory diseases, such as OA.

Ethics

All the animal experiments mentioned in the article have been approved by the Animal Protection Committee of the Fourth Military Medical University, Xi'an, Shaanxi, 710032, China. Animal welfare and experimental procedures were complied with the principles of Laboratory animal – Guidelines for ethical review of animal welfare (GB/T 35892–2018).

Acknowledgments

This work was financially supported by grants from the National Natural Science Foundation of China (81991504 and 81930025 to Yan Jin).

Disclosure

The authors report no potential conflicts of interest in this work.

References

1. Moon PM, Beier F. Novel insights into osteoarthritis joint pathology from studies in mice. *Curr Rheumatol Rep*. 2015;17(8):50.
2. Leifer VP, Katz JN, Losina E. The burden of OA-health services and economics. *Osteoarthritis Cartilage*. 2022;30(1):10–16.
3. Schulze-Tanzil G. Experimental therapeutics for the treatment of osteoarthritis. *J Exp Pharmacol*. 2021;13:101–125.
4. Lawson TB, Makela JTA, Klein T, Snyder BD, Grinstaff MW. Nanotechnology and Osteoarthritis. Part 2: opportunities for advanced devices and therapeutics. *J Orthop Res*. 2021;39(3):473–484.
5. Ferreira RM. Non-pharmacological and non-surgical interventions for knee osteoarthritis: asystematic review and meta-analysis. *acta reumatol port*. 2019;1:345.
6. Xiao L, Cui J, Sun Z, Liu Y, Zheng J, Dong Y. Therapeutic potential of nanotechnology-based approaches in osteoarthritis. *Front Pharmacol*. 2022;13:920824.
7. Shapouri-Moghaddam A, Mohammadian S, Vazini H, et al. Macrophage plasticity, polarization, and function in health and disease. *J Cell Physiol*. 2018;233(9):6425–6440.
8. Kapoor M, Martel-Pelletier J, Lajeunesse D, Pelletier JP, Fahmi H. Role of proinflammatory cytokines in the pathophysiology of osteoarthritis. *Nat Rev Rheumatol*. 2011;7(1):33–42.
9. Smith MD. The normal synovium. *Open Rheumatol J*. 2011;5:100–106.
10. Zhang H, Cai D, Bai X. Macrophages regulate the progression of osteoarthritis. *Osteoarthritis Cartilage*. 2020;28(5):555–561.
11. Kraus VB, McDaniel G, Huebner JL, et al. Direct in vivo evidence of activated macrophages in human osteoarthritis. *Osteoarthritis Cartilage*. 2016;24(9):1613–1621.
12. Raghu H, Lepus CM, Wang Q, et al. CCL2/CCR2, but not CCL5/CCR5, mediates monocyte recruitment, inflammation and cartilage destruction in osteoarthritis. *Ann Rheum Dis*. 2017;76(5):914–922.
13. Weinberg SE, Sena LA, Chandel NS. Mitochondria in the regulation of innate and adaptive immunity. *Immunity*. 2015;42(3):406–417.
14. Feno S, Munari F, Reane DV, et al. The dominant-negative mitochondrial calcium uniporter subunit MCUb drives macrophage polarization during skeletal muscle regeneration. *Sci Signal*. 2021;14(707):eabf3838.
15. Marchi S, Patergnani S, Missiroli S, et al. Mitochondrial and endoplasmic reticulum calcium homeostasis and cell death. *Cell Calcium*. 2018;69:62–72.
16. Wang Y, Li N, Zhang X, Horng T. Mitochondrial metabolism regulates macrophage biology. *J Biol Chem*. 2021;297(1):100904.
17. Williams NC, O'Neill LAJ. A role for the krebs cycle intermediate citrate in metabolic reprogramming in innate immunity and inflammation. *Front Immunol*. 2018;9:141.
18. Yan Y, Wei CL, Zhang WR, Cheng HP, Liu J. Cross-talk between calcium and reactive oxygen species signaling. *Acta Pharmacol Sin*. 2006;27(7):821–826.
19. Zhou Z, Ni K, Deng H, Chen X. Dancing with reactive oxygen species generation and elimination in nanotheranostics for disease treatment. *Adv Drug Deliv Rev*. 2020;158:73–90.
20. Raffaello A, De Stefani D, Sabbadin D, et al. The mitochondrial calcium uniporter is a multimer that can include a dominant-negative pore-forming subunit. *EMBO J*. 2013;32(17):2362–2376.
21. Zhou X, Yang W, Li J. Ca²⁺- and protein kinase C-dependent signaling pathway for nuclear factor-kappaB activation, inducible nitric-oxide synthase expression, and tumor necrosis factor-alpha production in lipopolysaccharide-stimulated rat peritoneal macrophages. *J Biol Chem*. 2006;281(42):31337–31347.
22. Angelova PR, Vinogradova D, Neganova ME, et al. Pharmacological sequestration of mitochondrial calcium uptake protects neurons against glutamate excitotoxicity. *Mol Neurobiol*. 2019;56(3):2244–2255.
23. Arduino DM, Perocchi F. Pharmacological modulation of mitochondrial calcium homeostasis. *J Physiol*. 2018;596(14):2717–2733.
24. Calvo-Rodriguez M, Bacskaï BJ. Mitochondria and calcium in Alzheimer's disease: from cell signaling to neuronal cell death. *Trends Neurosci*. 2021;44(2):136–151.
25. Cui C, Merritt R, Fu L, Pan Z. Targeting calcium signaling in cancer therapy. *Acta Pharm Sin B*. 2017;7(1):3–17.
26. Garbincius JF, Elrod JW. Mitochondrial calcium exchange in physiology and disease. *Physiol Rev*. 2022;102(2):893–992.
27. Gustafson HH, Holt-Casper D, Grainger DW, Ghandehari H. Nanoparticle uptake: the phagocyte problem. *Nano Today*. 2015;10(4):487–510.
28. Nogueira E, Gomes AC, Preto A, Cavaco-Paulo A. Folate-targeted nanoparticles for rheumatoid arthritis therapy. *Nanomedicine*. 2016;12(4):1113–1126.
29. Ummarino A, Gambaro FM, Kon E, Torres Andon F. Therapeutic manipulation of macrophages using nanotechnological approaches for the treatment of osteoarthritis. *Nanomaterials*. 2020;10:8.
30. Zhang YN, Poon W, Tavares AJ, McGilvray ID, Chan WCW. Nanoparticle-liver interactions: cellular uptake and hepatobiliary elimination. *J Control Release*. 2016;240:332–348.
31. Glasson SS, Blanchet TJ, Morris EA. The surgical destabilization of the medial meniscus (DMM) model of osteoarthritis in the 129/SvEv mouse. *Osteoarthritis Cartilage*. 2007;15(9):1061–1069.
32. Belosludtsev KN, Sharipov RR, Boyarkin DP, et al. The effect of DS16570511, a new inhibitor of mitochondrial calcium uniporter, on calcium homeostasis, metabolism, and functional state of cultured cortical neurons and isolated brain mitochondria. *Biochim Biophys Acta Gen Subj*. 2021;1865(5):129847.
33. Waldstein W, Perino G, Gilbert SL, Maher SA, Windhager R, Boettner F. OARS1 osteoarthritis cartilage histopathology assessment system: a biomechanical evaluation in the human knee. *J Orthop Res*. 2016;34(1):135–140.
34. Aitchison SM, Frentiu FD, Hurn SE, Edwards K, Murray RZ. Skin wound healing: normal macrophage function and macrophage dysfunction in diabetic wounds. *Molecules*. 2021;26(16):57.

35. Blom AB, van Lent PL, Holthuysen AE, et al. Synovial lining macrophages mediate osteophyte formation during experimental osteoarthritis. *Osteoarthritis Cartilage*. 2004;12(8):627–635.
36. Kim Y, Nurakhayev S, Nurkesh A, Zharkinbekov Z, Saparov A. Macrophage polarization in cardiac tissue repair following myocardial infarction. *Int J Mol Sci*. 2021;22(5):56.
37. Zhai Q, Chen X, Fei D, et al. Nanorepairers rescue inflammation-induced mitochondrial dysfunction in mesenchymal stem cells. *Adv Sci*. 2022;9(4):e2103839.
38. Im GI. Perspective on intra-articular injection cell therapy for osteoarthritis treatment. *Tissue Eng Regen Med*. 2019;16(4):357–363.
39. Toyoda E, Maehara M, Watanabe M, Sato M. Candidates for intra-articular administration therapeutics and therapies of osteoarthritis. *Int J Mol Sci*. 2021;22(7):45.
40. Utomo L, Fahy N, Kops N, et al. Macrophage phenotypes and monocyte subsets after destabilization of the medial meniscus in mice. *J Orthop Res*. 2021;39(10):2270–2280.
41. Lin C, Chen Z, Guo D, et al. Increased expression of osteopontin in subchondral bone promotes bone turnover and remodeling, and accelerates the progression of OA in a mouse model. *Aging*. 2022;14(1):253–271.
42. Loeser RF, Goldring SR, Scanzello CR, Goldring MB. Osteoarthritis: a disease of the joint as an organ. *Arthritis Rheum*. 2012;64(6):1697–1707.
43. Yuan XL, Meng HY, Wang YC, et al. Bone-cartilage interface crosstalk in osteoarthritis: potential pathways and future therapeutic strategies. *Osteoarthritis Cartilage*. 2014;22(8):1077–1089.
44. Berridge MJ, Bootman MD, Roderick HL. Calcium signalling: dynamics, homeostasis and remodelling. *Nat Rev Mol Cell Biol*. 2003;4(7):517–529.
45. Mattson MP, LaFerla FM, Chan SL, Leissring MA, Shepel PN, Geiger JD. Calcium signaling in the ER: its role in neuronal plasticity and neurodegenerative disorders. *Trends Neurosci*. 2000;23(5):222–229.
46. Paillusson S, Stoica R, Gomez-Suaga P, et al. There's something wrong with my MAM; the ER-mitochondria axis and neurodegenerative diseases. *Trends Neurosci*. 2016;39(3):146–157.
47. Schappe MS, Sztajn K, Stremaska ME, et al. Chanzyme TRPM7 mediates the Ca(2+) influx essential for lipopolysaccharide-induced toll-like receptor 4 endocytosis and macrophage activation. *Immunity*. 2018;48(1):59–74 e55.
48. Kang H, Zhang K, Wong DSH, Han F, Li B, Bian L. Near-infrared light-controlled regulation of intracellular calcium to modulate macrophage polarization. *Biomaterials*. 2018;178:681–696.
49. O'Neill LAJ, Artyomov MN. Itaconate: the poster child of metabolic reprogramming in macrophage function. *Nat Rev Immunol*. 2019;19(5):273–281.
50. Seegren PV, Downs TK, Stremaska ME, et al. Mitochondrial Ca(2+) signaling is an electrometabolic switch to fuel phagosome killing. *Cell Rep*. 2020;33(8):108411.
51. Sun X, Gao J, Meng X, Lu X, Zhang L, Chen R. Polarized macrophages in periodontitis: characteristics, function, and molecular signaling. *Front Immunol*. 2021;12:763334.

International Journal of Nanomedicine

Dovepress

Publish your work in this journal

The International Journal of Nanomedicine is an international, peer-reviewed journal focusing on the application of nanotechnology in diagnostics, therapeutics, and drug delivery systems throughout the biomedical field. This journal is indexed on PubMed Central, MedLine, CAS, SciSearch®, Current Contents®/Clinical Medicine, Journal Citation Reports/Science Edition, EMBase, Scopus and the Elsevier Bibliographic databases. The manuscript management system is completely online and includes a very quick and fair peer-review system, which is all easy to use. Visit <http://www.dovepress.com/testimonials.php> to read real quotes from published authors.

Submit your manuscript here: <https://www.dovepress.com/international-journal-of-nanomedicine-journal>